ARTICLE OPEN

Check for updates

Individual regional associations between Aβ-, tau- and neurodegeneration (ATN) with microglial activation in patients with primary and secondary tauopathies

Anika Finze[1,20], Gloria Biechele[1,2,20], Boris-Stephan Rauchmann[2,3], Nicolai Franzmeier[4,5,6], Carla Palleis[5,7,8], Sabrina Katzdobler[5,7,8], Endy Weidinger[7,8], Selim Guersel[9], Sebastian Schuster[1], Stefanie Harris[1], Julia Schmitt[1], Leonie Beyer[1], Johannes Gnörich[1], Simon Lindner[1], Nathalie L. Albert[1], Christian H. Wetzel[10], Rainer Rupprecht[10], Axel Rominger[1,11], Adrian Danek[7,8], Lena Burow[9], Carolin Kurz[9], Maia Tato[9], Julia Utecht[9], Boris Papazov[2,3], Mirlind Zaganjori[1,9], Lena-Katharina Trappmann[9], Oliver Goldhardt[12], Timo Grimmer[12], Jan Haeckert[13], Daniel Janowitz[4], Katharina Buerger[4], Daniel Keeser[3,9], Sophia Stoecklein[2], Olaf Dietrich[2], Estrella Morenas-Rodriguez[7], Henryk Barthel[14], Osama Sabri[14], Peter Bartenstein[1,5], Mikael Simons[5,7,15], Christian Haass[5,7,16], Günter U. Höglinger[7,8,17], Johannes Levin[5,7,8], Robert Perneczky[5,7,9,18,19] and Matthias Brendel[1,5,7]✉

β-amyloid (Aβ) and tau aggregation as well as neuronal injury and atrophy (ATN) are the major hallmarks of Alzheimer's disease (AD), and biomarkers for these hallmarks have been linked to neuroinflammation. However, the detailed regional associations of these biomarkers with microglial activation in individual patients remain to be elucidated. We investigated a cohort of 55 patients with AD and primary tauopathies and 10 healthy controls that underwent TSPO-, Aβ-, tau-, and perfusion-surrogate-PET, as well as structural MRI. *Z*-score deviations for 246 brain regions were calculated and biomarker contributions of Aβ (A), tau (T), perfusion (N1), and gray matter atrophy (N2) to microglial activation (TSPO, I) were calculated for each individual subject. Individual ATN-related microglial activation was correlated with clinical performance and CSF soluble TREM2 (sTREM2) concentrations. In typical and atypical AD, regional tau was stronger and more frequently associated with microglial activation when compared to regional Aβ (AD: $\beta_T = 0.412 \pm 0.196$ vs. $\beta_A = 0.142 \pm 0.123$, $p < 0.001$; AD-CBS: $\beta_T = 0.385 \pm 0.176$ vs. $\beta_A = 0.131 \pm 0.186$, $p = 0.031$). The strong association between regional tau and microglia reproduced well in primary tauopathies ($\beta_T = 0.418 \pm 0.154$). Stronger individual associations between tau and microglial activation were associated with poorer clinical performance. In patients with 4RT, sTREM2 levels showed a positive association with tau-related microglial activation. Tau pathology has strong regional associations with microglial activation in primary and secondary tauopathies. Tau and Aβ related microglial response indices may serve as a two-dimensional in vivo assessment of neuroinflammation in neurodegenerative diseases.

Molecular Psychiatry; https://doi.org/10.1038/s41380-023-02188-8

INTRODUCTION

Tauopathies account for the majority of neurodegenerative disorders. These include the secondary 3/4-repeat tauopathy Alzheimer's disease (AD) as the most prevalent form of dementia in societies with aging populations [1]. Primary tauopathies, such as Pick's disease, progressive supranuclear palsy (PSP), or corticobasal degeneration (CBD) are characterized by abnormal tau protein aggregation with three or four microtubule-binding-domains [2, 3]. However, regardless of the distinct neuropathology, there is also overlap in clinical phenotypes, for example, in corticobasal syndrome (CBS), which can be characterized by 3/4-repeat AD-like tau or 4-repeat tau (4RT) aggregation [4].

The neuropathological cascade of AD is characterized by the triad of accumulation of extracellular β-amyloid (Aβ) plaques,

[1]Department of Nuclear Medicine, LMU University Hospital, LMU Munich, Munich, Germany. [2]Department of Radiology, LMU University Hospital, LMU Munich, Munich, Germany. [3]NeuroImaging Core Unit Munich (NICUM), LMU University Hospital, LMU Munich, Munich, Germany. [4]Institute for Stroke and Dementia Research, Munich, Germany. [5]Munich Cluster for Systems Neurology (SyNergy), Munich, Germany. [6]Department of Psychiatry and Neurochemistry, Sahlgrenska Academy at the University of Gothenburg, Gothenburg, Sweden. [7]German Center for Neurodegenerative Diseases (DZNE), Munich, Germany. [8]Department of Neurology, LMU University Hospital, LMU Munich, Munich, Germany. [9]Department of Psychiatry and Psychotherapy, LMU University Hospital, LMU Munich, Munich, Germany. [10]Department of Psychiatry and Psychotherapy, University Regensburg, Regensburg, Germany. [11]Department of Nuclear Medicine, University Hospital, Inselspital Bern, Bern, Switzerland. [12]Department of Psychiatry and Psychotherapy, Klinikum Rechts der Isar, Technical University of Munich, School of Medicine, Munich, Germany. [13]Department of Psychiatry, Psychotherapy and Psychosomatics, Medical Faculty, University of Augsburg, Augsburg, Germany. [14]Department of Nuclear Medicine, University of Leipzig, Leipzig, Germany. [15]Institute of Neuronal Cell Biology, Technical University of Munich, Munich, Germany. [16]Chair of Metabolic Biochemistry, Biomedical Center (BMC), Faculty of Medicine, LMU Munich, Munich, Germany. [17]Department of Neurology, Hannover Medical School, Hannover, Germany. [18]Ageing Epidemiology (AGE) Research Unit, School of Public Health, Imperial College London, London, UK. [19]Sheffield Institute for Translational Neurosciences (SITraN), University of Sheffield, Sheffield, UK. [20]These authors contributed equally: Anika Finze, Gloria Biechele.
✉email: matthias.brendel@med.uni-muenchen.de

Received: 22 November 2022 Revised: 27 June 2023 Accepted: 10 July 2023
Published online: 26 July 2023

fibrillary tau aggregates in neurons, and microgliosis and astrogliosis [5–9]. In AD, this is conceptualized as the ATN sequence, where β-amyloidosis [A] is thought to precede and accelerate tau pathology [T] that leads to neurodegeneration [N] [10], now expanding towards an ATX(N) system, where X represents novel candidate biomarkers for additional pathophysiological mechanisms such as neuroimmune dysregulation, synaptic dysfunction or blood-brain-barrier alterations [11].

In AD and primary tauopathies, neuroinflammation represents an important mediator of protein aggregation and spread as well as disease progression, creating a positive feedback-loop in the disease cascade [12–15] and could serve as a valuable "X" parameter of ATX(N), then termed ATI(N). In this context, molecular imaging with 18 kDa translocator protein (TSPO) positron-emission-tomography (TSPO-PET) for stratification and monitoring of neuroinflammation could become crucial for targeting and assessing response to immunomodulatory therapies and has spurned the development of a wide range of tracers for human studies [16–19]. However, despite several studies with tau and TSPO tracers [20–22], ATI(N)-like schemes and interactions have only rarely been investigated in atypical AD or primary tauopathies, although Aβ copathology is common in 4RTs [23].

A detailed understanding of the pathophysiological interplay between the accumulation of misfolded proteins (i.e. Aβ and tau) and their contribution to neuroinflammation may provide deeper insight into mechanistic pathways [24]. In recent years, several multi-tracer studies in cohorts composed mainly of patients along the typical AD continuum revealed discrepant findings. Some investigations attributed the equal influence of Aβ and tau to microglial activation [25], while others supported the interaction of Aβ and microglia activation to set the pace for subsequent tau spread [12, 26]. The effects of microglial activation on cognition are thought to be strongly mediated by gray matter atrophy [27], and activated microglia have been correlated with parietal atrophy post mortem [28]. Thus, we aimed to investigate the interplay between ATI(N) biomarkers and microglial activation in a cohort composed of primary and secondary tauopathies, including atypical and typical AD. We analyzed the regional heterogeneity of ATI(N) biomarker alterations in tauopathies and we computed the partial contributions of ATN biomarkers to microglial activation at the individual patient level. Furthermore, we questioned the shape and magnitude of expurgated regional associations between aggregation of Aβ and tau with microglial activation. Finally, we correlated the individual Aβ- and tau-related microglial responses with clinical performance and cerebrospinal sTREM2 (soluble triggering receptor expressed on myeloid cells 2) levels.

MATERIAL AND METHODS

Study design

We enrolled patients with typical AD, AD-CBS, and 4RTs as well as healthy controls from ActiGliA, a prospective cohort study at Ludwig-Maximilians-University (LMU), approved by the local ethics committee (project-number 17-755; human PET analyses project-numbers 17-569, 19-022). Written informed consent was obtained from all participants in accordance with the Declaration of Helsinki. Requirements for inclusion were tau- and TSPO-PET, and T1w-MRI if available, within a time period of 18 months (mean time difference: 2.9 ± 4.4 months). Aβ-PET was tolerated up to 24 months prior to the remaining examinations (mean time difference: 6.7 ± 8.3 months). Tau-PET had to be conducted with dynamic emission recording to ensure the availability of the early-phase as an "N" biomarker. Patients with a low affinity TSPO binding status were assigned to a separate "LAB" study group regardless of their clinical diagnosis.

Patients with dementia, mild cognitive impairment (MCI), or subjective memory decline (SCD) due to AD were diagnosed according to the diagnostic criteria of the National Institute on Aging [29]. All patients with AD had a positive Aβ-PET scan and were allocated to the "typical AD" group. Clinical diagnosis of CBS was made as defined in the MDS-PSP criteria [30]. All enrolled CBS patients also fulfilled the Armstrong criteria of probable or possible CBD-CBS [31]. Only CBS patients with negative family history of Parkinson's disease and AD were included. The positivity or negativity of the Aβ-PET scan defined the allocation into "AD-CBS" or "4RT" study groups.

Group level TSPO-PET data of this cohort was previously published for patients with AD, 4RTs, and controls [32, 33]. Group level tau-PET data of this cohort was partially published for patients with AD, AD-CBS, 4RTs, and controls [21]. Group level data of early-phase imaging ([^{18}F]flutemetamol and [^{18}F]PI-2620) of parts of the cohort were previously published for AD-CBS and 4RTs [34, 35]. All reported data are unpublished.

PET imaging

PET data acquisition, reconstruction, and post-processing. For all PET procedures, including radiochemistry, acquisition, and pre-processing, we used an established and standardized protocol [21, 32, 35, 36]. Patients were scanned at the Department of Nuclear Medicine, LMU, using a Biograph 64 PET/CT scanner or a harmonized Biograph mCT (Siemens, Erlangen, Germany). In brief, [^{18}F]GE-180 TSPO-PET recordings (average dose: 179 ± 13 MBq) with an emission window of 60-80 min after injection were obtained to measure microglial activation [32]. [^{18}F]flutemetamol Aβ-PET recordings (average dose: 185 ± 16 MBq) with an emission window of 90-110 min after injection were performed for assessment of fibrillar Aβ accumulation [36]. Dynamic [^{18}F]PI-2620 tau-PET (average dose: 188 ± 15 MBq) with emission recording 0–60 min after injection was performed to quantify tau aggregation. Static frames of the perfusion phase (0.5–2.5 min) [35] and the late phase (20-40 min) [37] were reconstructed.

PET image analysis. Several established processing pipelines [21, 32, 34, 35, 37] were executed to ensure reproducibility by different analysis methodology. We performed all PET data analyses using PMOD (V3.9; PMOD Technologies LLC; Zurich; Switzerland). The primary analysis used static emission recordings which were coregistered to the Montreal Neurology Institute (MNI) space using non-linear warping (16 iterations, frequency cutoff 25, transient input smoothing 8 x 8 x 8 mm^3) to tracer-specific templates acquired in previous in-house studies [21, 32, 35, 36]. Given the strong binding differences between positive and negative Aβ-PET images, we used positive (number of subjects in the template: $n_t = 15$) and negative ($n_t = 27$) Aβ-PET templates after classification of the Aβ-status by a visual read by a single rater. A unified template was used for TSPO-PET ($n_t = 11$). Tau-PET images were coregistered to early (mixed [^{18}F]PI-2620 and [^{18}F]Flutemetamol; $n_t = 15$) [38] and late phase ($n_t = 28$) templates without distinction of tau-positivity.

Intensity normalization of all PET images was performed by calculation of standardized uptake value ratios (SUVr) using the cerebellum as an established pseudo-reference tissue for TSPO-PET [39]. The cerebellum was selected as the best compromise of a unified pseudo-reference tissue since it was also validated for [^{18}F]flutemetamol [40] and [^{18}F]PI-2620. To account for tau-positive areas in the cerebellum and to avoid spill-over of adjacent extracerebral structures, the dentate nucleus as well as superior and posterior layers of the cerebellum were excluded. Using the Brainnetome atlas [41], the brain was parcellated into 210 cortical and 36 subcortical volume-of-interests (VOIs), and standardized-uptake-value-ratios (SUVr) were calculated for all four PET read-outs. Per subject, the standardized regional deviation of SUVr (z-score) was calculated versus previously established age- and sex- matched normal cohorts for [^{18}F]flutemetamol (number of controls: $n_c = 13$, [34]), [^{18}F]GE-180 ($n_c = 13$, [42]), early [^{18}F]PI-2620 ($n_c = 14$, [43]) and late [^{18}F]PI-2620 ($n_c = 14$, [4]).

Structural MR imaging

Three-dimensional T1-weighted (T1w) MRI data were collected for the majority (60/72) of the cohort as reported previously [33]. The data were coregistered into the MNI standard space using the PNEURO tool (V3.9; PMOD Technologies LLC) and segmented into all 246 Brainnetome atlas VOIs. In this step, regional gray-matter-volumes (GMV), for analysis of possible brain atrophy, were collected. As described above, we used age- and sex- matched controls for the calculation of standardized *z*-scores ($n_c = 13$).

DNA extraction and SNP genotyping

Since the binding properties of second-generation TSPO ligands have been found to depend on genetic polymorphism of the TSPO gene [44, 45], all individuals underwent rs6971 single nucleotide polymorphism (SNP)

genotyping and were classified as low, medium, or high affinity binder (LAB, MAB or HAB). For this purpose, whole-blood samples were sent to the Department of Psychiatry of the University Hospital Regensburg for genotyping. Genomic DNA was extracted from 4 ml of whole blood using a QIAamp DNA Blood Maxi kit (Qiagen, Hilden, Germany) according to the manufacturer's protocol. DNA quality was assessed by optical absorbance and gel electrophoresis. Exon 4 of the TSPO gene and exon/intron junctions were amplified by PCR and sequenced using the Sanger method with the following primers: ex4-FAGTTGGGCAGTGGGACAG and ex4-R-CAGATCCTGCAGAGACGA. Sequencing data were analyzed using SnapGene software (GSL Biotech; http://snapgene.com).

sTREM2

sTREM2 concentrations were measured in all available CSF samples (4RT 14/26, AD-CBS 7/11, AD 10/18) by a modified assay based on the previously described sTREM2 ELISA using the MSD platform [46–48]. This assay was designed to selectively detect sTREM2 coming from the cleavage of the full-length protein. Prior to data analysis, the sTREM2 data were log-transformed.

Clinical assessments

As a part of the ActiGliA protocol, patients underwent comprehensive clinical examinations. Some of these data were used to compare ATN-related microglial activation with clinical performance. In this work, the PSP-rating scale (PSPRS: 0–100) [49], the motor-examination of the Movement Disorder Society revised form of the Unified Parkinson's Disease Rating Scale (UPDRS: 0 – 100) [50] and the Geriatric Depression Scale (GDS: 0–15) [51] were analyzed. In addition, the Montreal Cognitive Assessment scale (MoCA: 0–30) [52] and the Mini-Mental State examination (MMSE: 0–30) [53] were evaluated. For patients without MoCA but MMSE, the MMSE was converted to a comparable MoCA score [54]. For simplicity, other clinical performance data collected by ActiGliA are not further mentioned.

Statistics

For statistical calculations, SPSS (V25; IBM; Ehningen; Germany) and R (V4.1.2; R Core Team; 2021; Vienna; Austria) were used. Unless declared otherwise, the significance level was set to 0.05. The day of Tau-PET examination was used to define the age of the patients. Due to the lack of significant [^{18}F]GE-180 binding differences between individuals with MAB and HAB status [55], the rs6971-SNP status was not used as a covariate after the exclusion of individuals with LAB status.

Biomarker positivity classification. To assign patients to specific study groups, PET images were visually rated for Aβ-PET-positivity (single expert reader). In addition, an optimal cutoff based on a sensitivity / specificity tradeoff was defined for each of the 246 Brainnetome VOIs for each biomarker (excluding GMV) using single-region-ROC-analysis (cutoff: criterion of the point on the ROC curve closest to the point 0,1 [56, 57]). For semi-quantitative Aβ-PET we defined the threshold to best discriminate the AD groups (AD-CBS and typical AD) from 4RT and CTRL. For TSPO-PET, tau-PET, and perfusion, the optimal cutoff was determined to discriminate 4RT, AD-CBS, and AD against CTRL. For every patient and biomarker, we summed up the positivity of the five regions with the highest area-under-curve (AUC) values and calculated another optimal cutoff via roc analysis to finally declare a patient as biomarker positive or negative.

Demographics, clinical performance, and sTREM2. To test for group differences in demographic data, a 1-way analysis of variance (ANOVA) was used for age, sTREM2, and MoCA. Sex and rs6971-SNP were subject to a chi-square (χ^2) test. With significant ANOVA or χ^2-test, multiple posthoc unpaired two-tailed Student's *t*-tests were subsequently performed between all groups (unadjusted for multiple testing).

Multiregion analyses. A descriptive heatmap was created by calculating arithmetic means ($\bar{x}$) within 24 composed Brainnetome regions [58] from the acquired *z*-scores and displayed in color scale per patient group and biomarker. Thereby, all $\bar{x} > 2$ were set equal to 2, and all $\bar{x} < -2$ were set equal to −2. For each of the 24 composite regions, the frequency of patients with peak *z*-scores (highest *z*-score along all 24 regions) was determined and visualized relative to the total amount of patients per group. These arithmetic means and biomarker peak distributions of the 24 brain regions were then tested for intercorrelations between those biomarkers (4RT, AD-CBS, and AD pooled) using linear Pearson's correlation (r).

Regression models. For each subject, a multiple linear regression model was defined to analyze the influence of the independent ATN variables (Aβ A, Tau T, Perfusion N1, GMV N2) on microglial activity (I), taking all 246 Brainnetome VOIs into account. The obtained standardized β-coefficients of ATN were visualized by a combined violin-box-plot. Within each diagnosis group, the β-coefficients of the four independent variables were tested for group differences using ANOVA with age and sex as covariates. Multiple post-hoc tests (dichotomous ANOVA, age, and sex corrected) were performed if there was a significant group difference. False discovery rate (FDR, six tests) correction to decrease the risk of α-error-accumulation was applied. Furthermore, each *p*-value was Bonferroni adjusted for a total of five diagnostic groups.

As a supplementary analysis, similar to the methodology explained before, we ordered all β-values from the single-patient regression per biomarker and tested for group differences between the five diagnostic groups. Post-hoc analysis and correction for multiple testing were performed using FDR (ten tests) and Bonferroni (four biomarkers). To analyze the influence of ATN on microglial activity at the group level, multivariate linear regression models (covariates: age, sex, subject-ID, and all other ATN biomarkers) were applied (including all 246 Brainnetome VOI z-scores of all patients per group). Partial regressions were analyzed and fitted values were used to classify a VOI as biomarker positive or negative. For ATN, the z-score cutoff for the classification of positivity was determined at >2 (AT) and <−2 (N). The *z*-score cutoff of I was set >0, to ensure inclusion of regions with low-level inflammation above the average of controls. Proportions of I+ A+ / I+ T+ / I+ N+ to the total amount of A+ / T+ / N+ VOIs were calculated.

Correlation and interaction analyses. Spearman's rank correlation (r_s) was used to analyze the relationship of clinical parameters and sTREM2 with AT-related microglial activation, in a cohort of composed 4RT, AD-CBS, and AD patients. Correlation analyses were adjusted for sex, age, global-patient-TSPO-load (mean *z*-scores of 246 VOIs), and global-patient-AT-load (mean *z*-scores of 246 VOIs of the respective biomarker). When significant correlations were observed, individual correlation sub-analyses were conducted within 4RT and AD (AD, AD-CBS). For sTREM2, we primarily separated the cohort into a group with AD-pathology (AD-CBS, AD) and a group with 4R-tauopathies. No correction for multiple testing due to the exploratory character was applied in these analyses. Subsequently, A and T were tested for interaction effects.

RESULTS

Demographics

The analyzed cohort consisted of 26 patients with 4RTs, 11 patients with AD-CBS, 18 patients with typical AD, 7 mixed LABs, and 10 controls who received examinations with all ATN imaging biomarkers (Table 1). Age, sex, and sTREM2 did not differ between subgroups of the cohort. A significant group difference for rs6971 SNP status was identified (4RT: MAB/HAB = 7/18, AD-CBS: MAB/HAB = 5/6, AD: MAB/HAB = 8/8, CTRL: MAB/HAB = 7/2, $\chi^2 = 8.575$, $p = 0.036$). The MoCA scores of the controls were found to be significantly higher than those of 4RT, AD-CBS, and AD. AD-CBS showed significantly lower MoCA scores than 4RT and AD (4RT: 22.8 ± 4.6, AD-CBS: 17.6 ± 6.6, AD: 22.4 ± 6.2, LAB: 22.0 ± 7.5, CTRL: 28.6 ± 1.6, F = 5.175, $p = 0.001$). Further demographic statistics are displayed in Table 1. Demographics of larger tracer specific control cohorts that were used for the calculation of individual *z*-scores are reported in Supplemental Table 1.

Strong regional heterogeneity of ATN biomarker alterations in primary and secondary tauopathies

First, we investigated regional alterations of microglial activity, Aβ, tau, perfusion, and GMV in our cohort of primary (4RT) and secondary (typical AD, AD-CBS) tauopathies at the group level. Frequencies of overall biomarker positivity across subgroups are illustrated in Fig. 1A. As expected from previous studies [4, 21] we found the highest levels of Aβ-PET and tau-PET signals in cortical brain regions of patients with typical and atypical AD, whereas

Table 1. Demographics.

Table 1	Neurodegenerative disease				Controls	ANOVA / χ^2
	4RT	AD-CBS	AD	LAB	CTRL	F (*p*-value)
n	26	11	18	7	10	
Age (years)	70.8 ± 6.3	75.7 ± 5.5	70.7 ± 7.4	75.0 ± 6.5	69.5 ± 8.9	1.781 (0.143)
Sex	♀ 13 / ♂ 13	♀ 7 / ♂ 4	♀ 9 / ♂ 9	♀ 2 / ♂ 5	♀ 7 / ♂ 3	3.492 (0.479)
rs6971 SNP	MAB: 7	MAB: 5	MAB: 9		MAB: 8	8.575 (0.036)
	HAB: 19	HAB: 6	HAB: 9		HAB: 2	
	(*n* = 26)	(*n* = 11)	(*n* = 18)		(*n* = 10)	
sTREM2	0.969 ± 0.138	1.012 ± 0.108	0.955 ± 0.088	0.981 ± NA	1.009 ± 0.094	0.388 (0.816)
	(*n* = 14)	(*n* = 7)	(*n* = 10)	(*n* = 1)	(*n* = 6)	
MoCA	22.8 ± 4.6	17.6 ± 6.6	22.4 ± 6.2	22.0 ± 7.5	28.6 ± 1.6	5.175 (0.001)
	(*n* = 24)	(*n* = 10)	(*n* = 14)	(*n* = 3)	(*n* = 9)	

Posthoc *p*-value MoCA	4RT	AD-CBS	AD	LAB
AD-CBS	0.011			
AD	0.838	0.0315		
LAB	0.807	0.209	0.898	
CTRL	0.007	< 0.001	0.008	0.067

Data are presented as mean ± standard deviation and number of frequency (*n*). Demographics were statistically tested by ANOVA or chi-square (χ^2) test. With significant ANOVA group difference, multiple unpaired two-tailed Student's *t*-tests were performed.

AD Alzheimer's disease, *AD-CBS* corticobasal syndrome with AD-pathology, *4RT* four-repeat tauopathies, *LAB* low affinity binder, *MAB* medium affinity binder, *HAB* high affinity binder, *CTRL* healthy controls, *ANOVA* analysis of variance, χ^2 chi-square, *MoCA* Montreal-Cognitive-Assessment-Scale, *MMSE* Mini-Mental State Examination, *sTREM2* soluble triggering receptor expressed on myeloid cells 2.

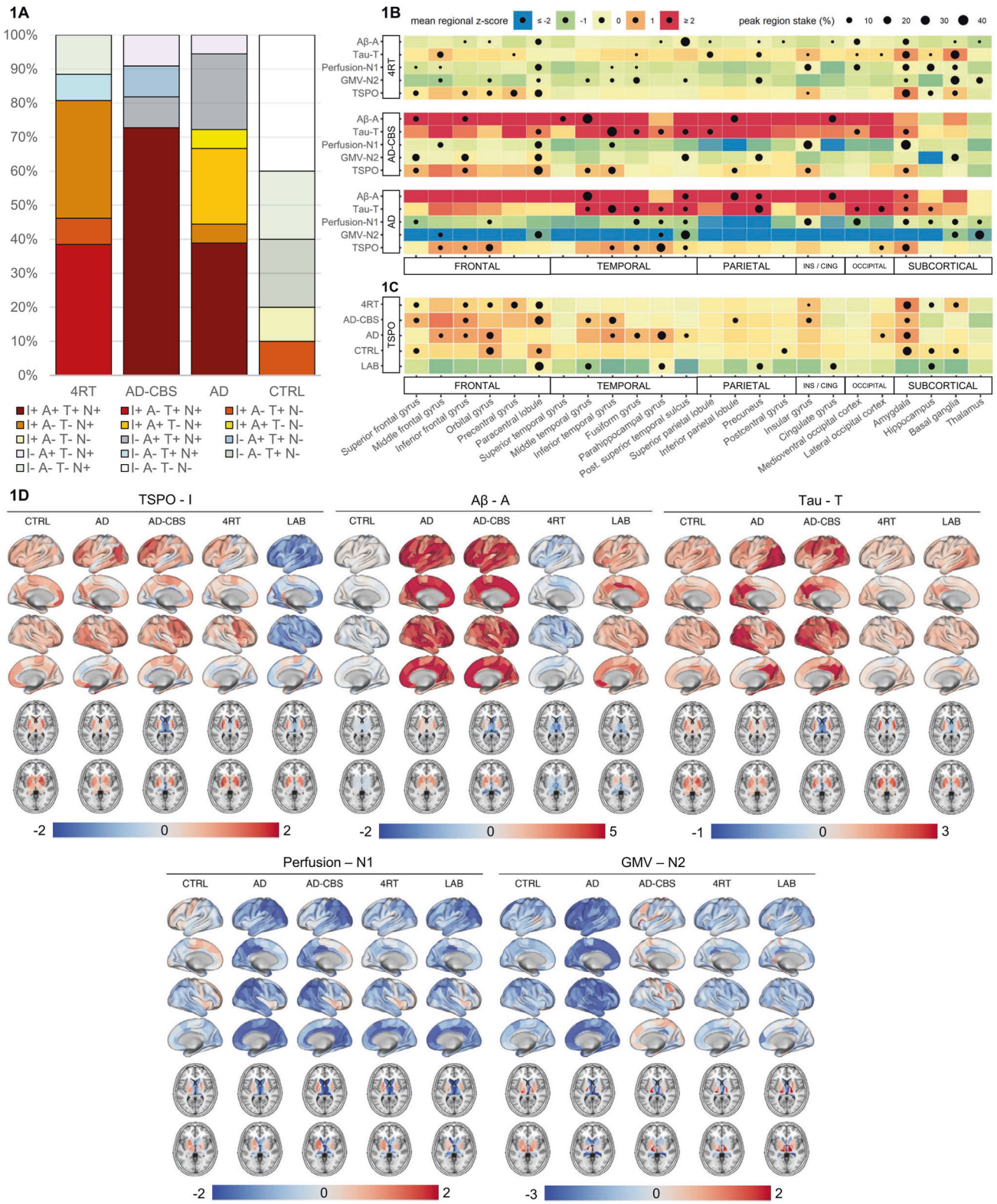

patients with 4RTs showed low Aβ-PET levels and subcortical predominance of tau accumulation (Fig. 1B). TSPO-PET signal increases were abundantly observed in tau-, but not Aβ-PET positive brain regions (tau-TSPO: $r = 0.312$, $p = 0.008$ / Aβ-TSPO: $r = 0.071$, $p = 0.552$). Regional peak distribution of "N" biomarkers followed the individual patterns of tau- (tau-perfusion: $r = 0.246$, $p = 0.037$ / tau-atrophy: $r = 0.270$, $p = 0.022$), but not Aβ-PET (Aβ-perfusion: $r = -0.023$, $p = 0.851$ / Aβ-atrophy: $r = 0.035$, $p = 0.771$). TSPO-PET levels were distinctly higher in primary and secondary tauopathies with MAB and HAB status when compared to a mixed cohort ($n = 2$ AD, $n = 4$ 4RT, $n = 1$ healthy control) of low-affinity binders (Fig. 1C).

Importantly, we found a scattered distribution of individual ATN peak regions within subgroups of primary and secondary

Fig. 1 Determination of ATI(N) biomarker positivity and ATI(N) biomarker heterogeneity using a multiregional analysis. A Overall ATI(N) biomarker positivity of all included subjects for I(TSPO)-, A(Aβ)-, T(tau)- and N(perfusion, early tau)-PET at the group level. Single-region-ROC-analyses were applied to identify regions ($n = 5$) that discriminate best among the study groups (maximum area-under-curve) for each biomarker. For each region an individual cutoff was set based on a sensitivity/specificity tradeoff and patients were classified as biomarker-positive or –negative based on the averaged regions that allowed the most optimal discrimination. Please note that AD also includes AD pathological change according to NIA-AA. **B** Heterogeneity of regional ATI(N) biomarker peak distribution. The heatmap was determined by calculating arithmetic means ($\bar{x}$) within 24 composed brain regions (from *z*-scores) and displayed in color scale. All $\bar{x} > 2$ were set equal to 2 and all $\bar{x} < -2$ were set equal to −2. The brain region with the highest *z*-score was determined for each study participant and the peak region frequency was plotted proportionally (%) to the number of patients in one group. **C** Comparison of TSPO-PET levels in patients with primary and secondary tauopathies and medium- and high-affinity TSPO binding status when compared to a mixed cohort ($n = 2$ AD, $n = 4$ 4RT, $n = 1$ healthy control) of individuals with low-affinity TSPO binding status using the same methodological approach as in (**B**). **D** Regional ATI(N) biomarker PET signal alterations at the group level. Within each study group, the mean *z*-score of each Brainnetome region was calculated and plotted as surface projections (lateral and medial view) and axial slices of the basal ganglia. AD Alzheimer's disease, AD-CBS corticobasal syndrome with AD-pathology, 4RT four-repeat tauopathies, LAB low affinity binder, CTRL healthy controls, TSPO 18-kDa translocator protein, Aβ β-amyloid, GMV gray-matter-volume, PET positron-emissions-tomography, ROC receiver-operating-characteristic.

tauopathy subgroups (Fig. 1D). Highest Aβ-PET *z*-scores in individual patients with typical AD were observed in temporal (44.4%) and parietal lobe (33.3%), as well as cingulate gyrus (16.7%) and amygdala (5.6%), whereas individual patients with AD-CBS had highest Aβ-PET *z*-scores in the middle and superior temporal gyrus (45.5%), parietal lobe (18.2%), cingulate (18.2%) and frontal cortices (18.2%). As expected from previous work [4], the highest individual tau-PET alterations in patients with 4RTs were observed in the basal ganglia (26.9%), but heterogeneity of peak signal alterations was observed with involvement of limbic regions (23.1%), parietal (19.2%), frontal (15.4%) and temporal (3.8%) cortices. In line with previous pattern classification [59], we found various peak regions of individual tau-PET not only in AD-CBS but also in typical AD, with a predominance of temporal regions (50.0%) but peaks in the precuneus (22.2%), occipital cortices (16.7%) as well as limbic regions (11.1%).

Regional Tau-PET is closely associated with the individual microglia response in primary and secondary tauopathies

Given the strong regional heterogeneity of Aβ and tau accumulation in primary and secondary tauopathies, we applied a multiregional regression model to investigate the detailed associations of ATN biomarker alterations with microglia activation at the individual patient level (Fig. 2A). In 4RTs, Tau-PET contributed significantly to the regional explanation of TSPO-PET ($\beta_T = 0.418 \pm 0.154$ / $p < 0.001$ in 88% of individuals), whereas Aβ-PET did not ($\beta_A = -0.030 \pm 0.124$ / $p < 0.001$ in 15% of individuals; Fig. 2B/C). Perfusion ($\beta_{N1} = 0.218 \pm 0.176$ / $p < 0.001$ in 54% of individuals) and GMVs ($\beta_{N2} = 0.026 \pm 0.108$ / $p < 0.001$ in 12% of individuals) were associated with regional TSPO-PET in individuals with 4RTs but did not exceed controls at the group level (Supplemental Fig. 1). The positive character of these regional associations suggested an unspecific coupling of regional tracer signals by perfusion and atrophy. Within the 4RT subgroup, the explanation of TSPO-PET alterations by tau-PET distinctly exceeded the explanation by "A" and "N" biomarkers (Fig. 2B).

In patients with AD-CBS and typical AD, we observed a significant explanation of regional TSPO-PET by Aβ-PET (AD-CBS: $\beta_A = 0.131 \pm 0.186$ / $p < 0.001$ in 64% of individuals; AD: $\beta_A = 0.142 \pm 0.123$ / $p < 0.001$ in 33% of individuals) and tau-PET (AD-CBS: $\beta_T = 0.385 \pm 0.176$ / $p < 0.001$ in 82% of individuals; AD: $\beta_T = 0.412 \pm 0.196$ / $p < 0.001$ in 83% individuals; Fig. 2B/C), but explanation by perfusion and GMVs did again not exceed the level of controls (Supplemental Fig. 1). Tau-PET indicated the strongest regional relations with TSPO-PET in both AD groups among all ATN biomarkers (Fig. 2B).

In the subgroup of mixed LABs, we did not observe a significant explanation of the TSPO-PET signal by ATN biomarkers ($p = 0.420$). Associations between tau-PET and Aβ-PET with TSPO-PET were obliterated in individual cases with LAB status (Supplemental Fig. 2). Noteworthy, the individual positive associations between perfusion and TSPO-PET were still present for cases with LAB status, pinpointing the unspecific regional association between perfusion and TSPO uptake patterns when the tracer cannot bind the target.

Incremental tau aggregation is associated with high regional activation of microglia

To test for regional associations between ATN biomarkers and microglia activation at the disease level, we applied a partial regression model to study the specific association of single ATN parameters with TSPO-PET, controlled for all other ATN biomarkers, age, sex, and subject-ID.

When pooling VOI-specific data across 4RT subjects (26 patients with 246 Brainnetome VOIs), 6396 analyzed brain regions revealed high proportions of TSPO-positive (I+) regions among T+ (82%) but a low proportion of TSPO-positive regions among A+ (48%) and N+ (27%) regions (Fig. 3A). There was a weak partial association between regional Aβ ($\beta = 0.030$, $p = 0.011$) with TSPO but a strong partial association between regional Tau and TSPO ($\beta = 0.381$, $p < 0.001$; Fig. 3A). The partial association between perfusion and TSPO ($\beta = 0.270$, $p < 0.001$) was driven by lower TSPO-PET signals in regions with strong decreases in perfusion (Fig. 3A).

Both AD cohorts (2706 analyzed regions of AD-CBS and 4428 analyzed regions of typical AD) revealed similar partial associations between regional ATN biomarker alterations and TSPO-PET. There was a weak but significant regional association between Aβ and TSPO in patients with AD-CBS ($\beta = 0.117$, $p < 0.001$) and typical AD ($\beta = 0.117$, $p < 0.001$; Fig. 3B/C). Regional tau again appeared as the strongest driver of TSPO-PET signals in AD-CBS ($\beta = 0.357$, $p < 0.001$) and typical AD ($\beta = 0.412$, $p < 0.001$) with high proportions of regional TSPO-PET positivity in regions with significant tau accumulation (AD-CBS: 81%, typical AD: 79%; Fig. 3B/C). Perfusion indicated a significant association with TSPO-PET signals for both AD subgroups (Fig. 3B/C). Controls validated the applied thresholds of ATN positivity and indicated only a few A+, T+, and N+ regions (Fig. 3D).

Associations of Aβ- and tau-associated microglial response with clinical performance and sTREM2

Finally, we tested if individual associations between Aβ and tau with microglial activation were correlated with indices of clinical severity and sTREM2. The rationale was to investigate if specific "A" or "T" associated microglial activation can be linked to improved or deteriorated clinical performance. Tau associated microglial activation revealed a general association with worse clinical performance (Fig. 4). Patients indicated more depressive symptoms ($r_s = 0.460$, $p = 0.011$) and worse results on the UPDRS scale ($r_s = 0.503$, $p = 0.006$), when patients had high associations between regional tau and microglial activation. We observed a significant interaction effect between Aβ and tau associated

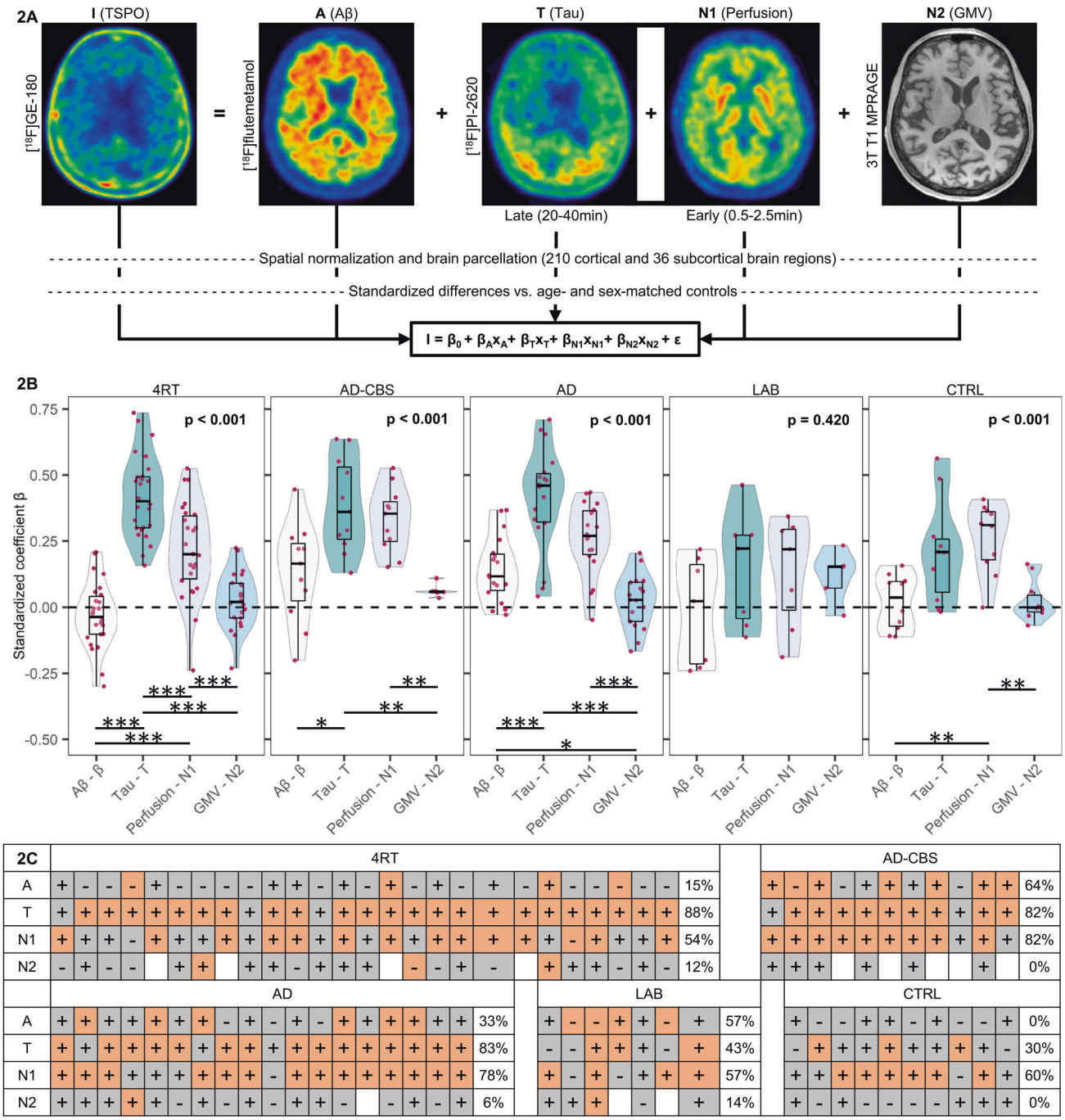

2C

	4RT																									
A	+	-	-	-	+	-	-	-	-	+	+	-	+	-	+	-	+	-	+	-	+	-	-	-	-	-	15%
T	+	+	+	+	+	+	+	+	+	+	+	+	+	+	+	+	+	+	+	+	+	+	+	+	+	+	88%
N1	+	+	+	-	+	+	+	+	+	+	+	+	+	+	+	+	+	+	+	+	-	+	+	+	+	+	54%
N2	-	+	-	-		+	+		+	+	-	+	+	+			-	-	+	-		+	+	+	-	+	-	12%

	AD-CBS											
A	+	-	+	-	+	+	+	+	-	+	+	64%
T	+	+	+	+	+	+	+	+	+	+	+	82%
N1	+	+	+	+	+	+	+	+	+	+	+	82%
N2	+	+	+		+		+			+		0%

	AD																									
A	+	+	+	+	+	+	+	-	+	-	+	-	+	+	+	+	+	+	+	+	+	+	+	+	+	+	33%
T	+	+	+	+	+	+	+	+	+	+	+	+	+	+	+	+	+	+	+	+	+	+	+	+	+	+	83%
N1	+	+	+	+	+	+	+	+	+	-	+	+	+	+	+	+	+	+	+	+	+	+	+	+	+	+	78%
N2	+	+	+	+	+	-	+	-	+	-	+	+	-		-	+	-	+	+	+		-		+	+	+	6%

	LAB																									
A	+	-	-	+	+	-	+	57%																		
T	-	-	+	+	+	-	+	43%																		
N1	+	-	+	-	+	+	+	57%																		
N2	+	+	+		-		+	14%																		

	CTRL																									
A	+	-	-	+	+	-	+	-	-	+	0%															
T	-	+	+	+	+	+	+	+	+	-	30%															
N1	+	+	+	+	+	+	+	-	+	+	60%															
N2	+	-	+	-	-	-	-	+	+	+	0%															

Fig. 2 Multiregional regression analysis to determine the association of ATN biomarkers with microglial activation at the individual patient level. A Methodological workflow: PET and MRI data were spatial normalized to tracer specific templates acquired in previous in house studies (Montreal Neurology Institute (MNI) space) and parcellated into 210 cortical and 36 subcortical brain regions. PET-tracer uptake and gray-matter-volumes (GMV, from MRI) were transformed into *z*-scores with age- and sex-matched controls. **A** multiple linear regression model was performed ($I = \beta_0 + \beta_A x_A + \beta_T x_T + \beta_{N1} x_{N1} + \beta_{N2} x_{N2} + \varepsilon$) at the single-patient-level and standardized coefficients (β) were derived for each ATN biomarker. **B** β-coefficients were visualized as a combined violin-box-plot and show the association of ATN biomarkers with microglia activation, each dot representing a single subject. Within each diagnosis group, the β-coefficients of the four independent variables were tested for group differences using ANOVA with age and sex as covariates. Multiple posthoc tests (dichotomous ANOVA, age, and sex corrected) were performed if there was a significant group difference. Combined false discovery rate (FDR, six *p*-values) and Bonferroni (five p-values) correction were applied to decrease the risk of α-error-accumulation. *$p < 0.05$, **$p < 0.01$, ***$p < 0.001$. **C** Heatmap indicates the significance of ATN biomarker contribution to microglia activation resulting from the regression analysis in different diagnostic subgroups. Orange: $p < 0.001$. Gray: $p \geq 0.001$. The percentage was calculated as the proportion of significant regression models of patients, relative to the total number of patients in the diagnostic group. Plus and minus signs were used to indicate the positivity or negativity of the associated β-coefficients. AD Alzheimer's disease, AD-CBS corticobasal syndrome with AD-pathology, 4RT four-repeat tauopathies, LAB low affinity binder, CTRL healthy controls, TSPO 18-kDa translocator protein, Aβ β-amyloid, GMV gray-matter-volume, PET positron-emissions-tomography, MRI magnetic-resonance-imaging, MNI Montreal Neurology Institute, ANOVA analysis of variance, FDR false discovery rate.

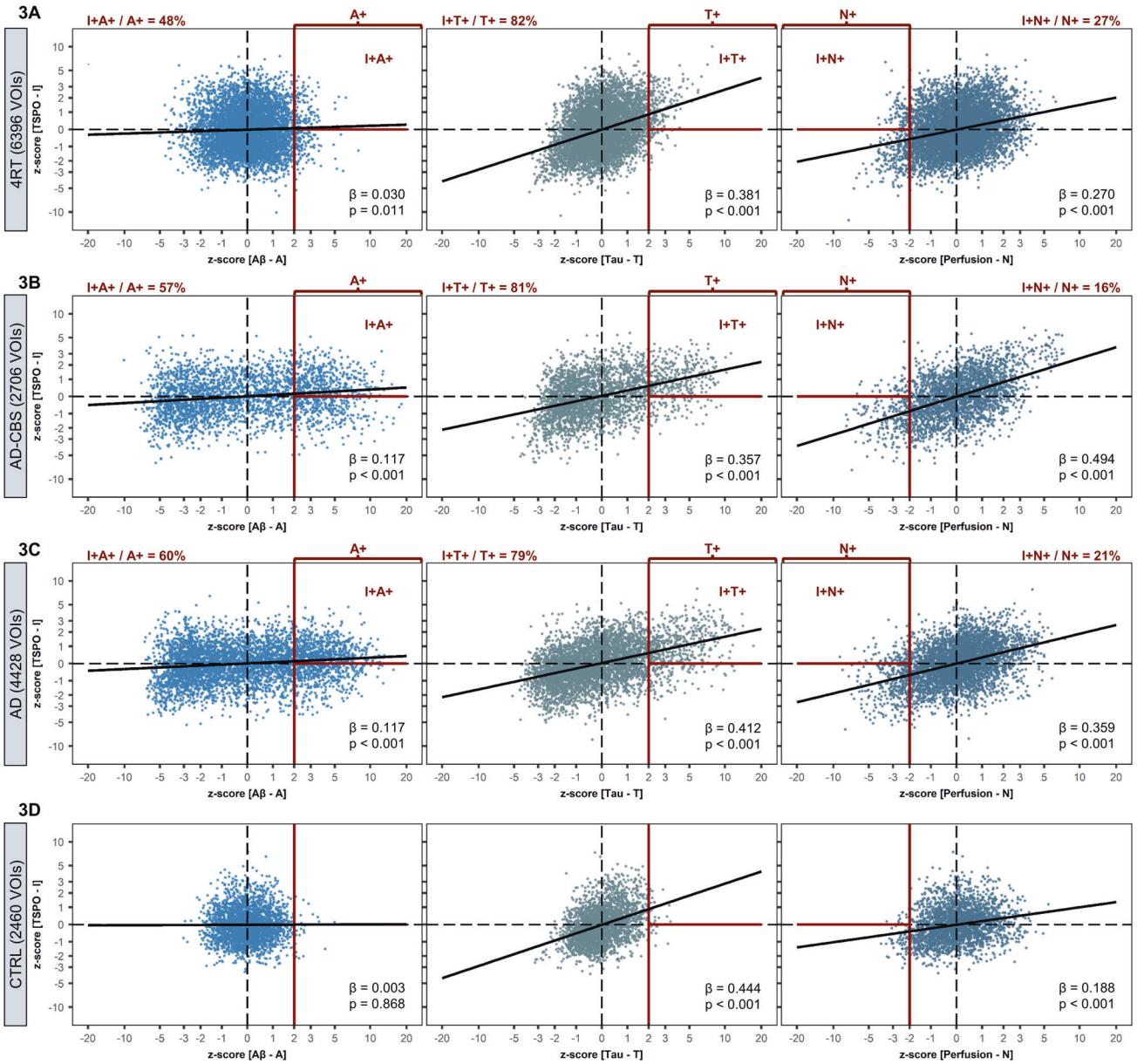

Fig. 3 Multiregional regression analysis to determine the association of ATN biomarkers with microglial activation at the group level. A multiple linear regression model was performed ($I = \beta_0 + \beta_A x_A + \beta_T x_T + \beta_N x_N + \text{age} + \text{sex} + \text{subject-ID} + \varepsilon$) at group-level for (**A**) 4RT, (**B**) AD-CBS, (**C**) AD, and (**D**) CTRL using z-scores of all single regions of all individuals combined. The standardized coefficient (β) and the associated *p*-value were calculated. Fitted values of the partial regressions were used to classify a VOI as biomarker positive or negative. For ATN, the *z*-score cutoff for the classification of positivity was determined at >2 (AT) and <−2 (N). The *z*-score cutoff of I was set >0. Proportions of I+ A+ / I+ T+ / I+ N+ to the total amount of A+ / T+ / N+ VOIs were calculated. AD Alzheimer's disease, AD-CBS corticobasal syndrome with AD-pathology, 4RT four-repeat tauopathies, CTRL healthy controls, TSPO 18-kDa translocator protein, Aβ β-amyloid.

microglial activation for UPDRS ($T = 2.401$, $p = 0.019$) and GDS ($T = 3.581$, $p < 0.001$), suggesting that microglial response to different protein aggregation may have opposite effects on brain function and clinical severity. Significant correlations were further examined to determine whether they were driven by a specific patient subgroup. The correlation of tau-associated microglial activation with GDS appeared to be driven by the AD cohort (4RT: $r_s = 0.354$, $p = 0.150$; AD + AD-CBS: $r_s = 0.758$, $p = 0.029$), whereas the correlation between tau-associated microglial activation and UPDRS appeared to be driven by the 4RT cohort (4RT: $r_s = 0.593$, $p = 0.007$; AD + AD-CBS: $r_s = -0.698$, $p = 0.190$). There were no correlations, nor interaction effects for MoCA or PSPRS. The AD-group showed a significant interaction effect when Aβ-associated TSPO-PET signals and tau-associated TSPO-PET signals were correlated with sTREM2 ($T = 2.732$, $p = 0.011$; Fig. 5). This indicated that high Aβ-TSPO associations but low tau-TSPO associations are linked with sTREM2 increases at the individual patient level. Contrary, patients with 4RT showed high sTREM2 levels when regional TSPO-PET was associated with tau-PET ($r_s = 0.705$, $p = 0.034$), which may indicate different trajectories of microglia phenotypes in the course of primary and secondary tauopathies.

DISCUSSION

We provide the first study that uses a regional resolution of ATI(N) PET and grey matter volumes in a combined cohort of primary and secondary tauopathies to investigate the detailed associations between the accumulation of misfolded proteins, perfusion, and

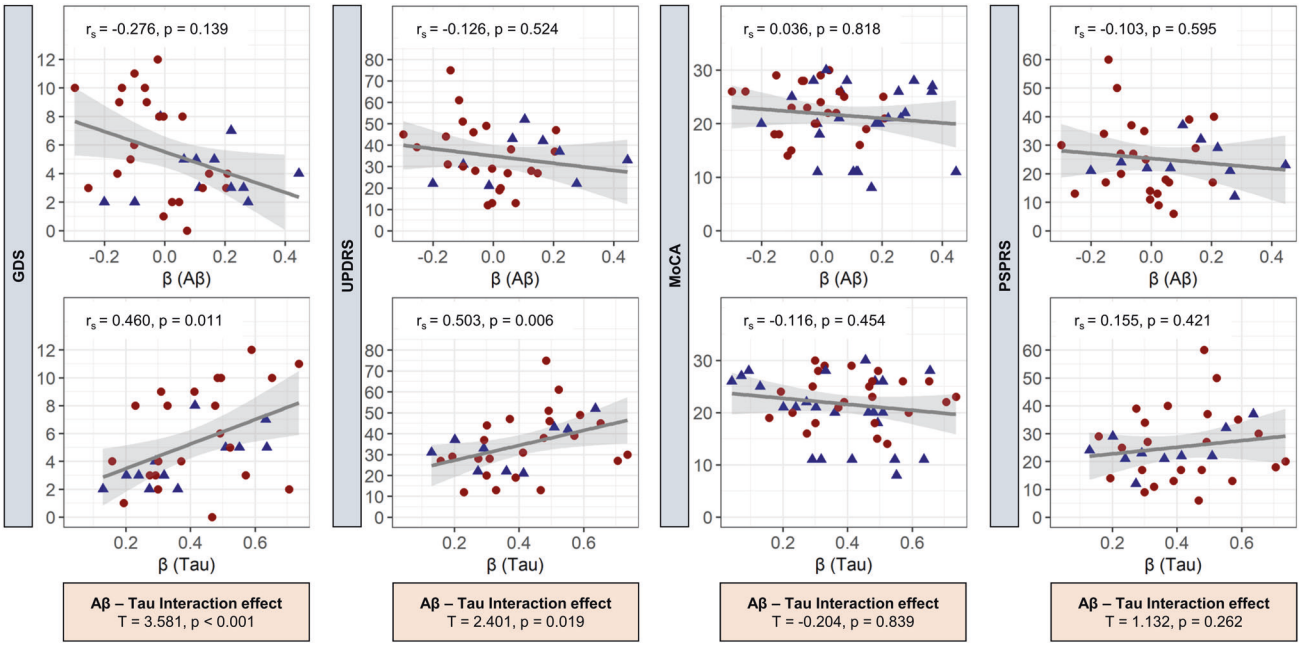

Fig. 4 Correlation of AT associated microglial activation with clinical performance. Standardized coefficients β (single patient regression), to detect Aβ (A)- and tau (T)- associated microglial activation, were correlated with clinical performance scores (Spearman's correlation coefficient, r_s). For statistical calculations, 4RT, AD-CBS, and AD were pooled. ● = 4RT, ▲ = AD-CBS + AD. Correlation analyses were adjusted for sex, age, global-patient-TSPO-load (mean z-scores of 246 VOIs), and global-patient-AT-load (mean *z*-scores of 246 VOIs of the respective biomarker). No correction for multiple testing was applied. Subsequently, A and T were tested for interaction effects. AD Alzheimer's disease, AD-CBS corticobasal syndrome with AD-pathology, 4RT four-repeat tauopathies, LAB low affinity binder, CTRL healthy controls, TSPO 18-kDa translocator protein, Aβ β-amyloid, GMV gray-matter-volume, MoCA Montreal-Cognitive-Assessment-Scale, MMSE Mini-Mental State Examination, UPDRS Unified-Parkinson's-Disease-Rating-Scale (motor part), PSPRS Progressive-Supranuclear-Palsy-Rating-Scale, GDS Geriatric-Depression-Scale.

volume changes with microglial activation. We find distinct heterogeneity of regional distribution patterns of ATI(N) biomarkers among patients with tauopathies. Regional accumulation of tau was the strongest predictor of microglial activation in individual patients with primary and secondary tauopathies, whereas Aβ, perfusion, and gray matter volumes indicated only weaker associations with regional TSPO-PET. Individual associations between ATN biomarkers and microglial activation were abrogated in low-affinity binders, demonstrating in vivo specificity of [^{18}F]GE-180 to TSPO. Finally, we obtained preliminary evidence of worse clinical performance when microglial activation was associated with tau at the individual patient level.

The major finding of our study revealed that, among all ATN biomarkers, aggregated tau has the closest link with colocalized microglia activation in primary tauopathies and AD. Thus, our study confirmed joint accumulation of tau and microglial activation in typical AD [12] and adds evidence of similar regional trajectories in 4RTs and atypical AD. Several clinical and preclinical investigations indicated that both Aβ and tau are closely related to PET and histological measurements of increased microglial activity [12, 15, 25, 60–62]. However, the detailed interplay between ATN biomarkers and neuroinflammation was discussed controversially. Even at the stage of single ATN biomarkers, distinct subtypes of microglia activation have been shown to occur in response to Aβ accumulation, depending on disease stage [63]: a protective neuroinflammatory response that could be beneficial due to phagocytosis of neurotoxic Aβ species, and a detrimental one with negative effects that leads to inhibition of synaptic functioning and increased cell death [63, 64]. Furthermore, atrophy was found to mediate the effects of both tau pathology and neuroinflammation on cognition in AD [27]. We hypothesized that regression models of multiple biomarkers in different brain regions could deepen the understanding of the ATI(N) biomarker interplay with I as an index of microglial activation. The application of this approach at the individual patient level enabled us to directly compare the partial influence of ATN biomarkers and we clearly observed a stronger association between regional aggregation of tau with microglial activation than did Aβ deposits. This finding could be related to exhausted microglia at advanced stages of Aβ accumulation [65]. Patients with typical and atypical AD showed a significant influence of regional Aβ on microglial activation but this association was not found in 4RTs. This is of particular interest since subthreshold levels of Aβ occur in 4RTs [66] but do not have a major impact on neuroinflammation according to our data.

With regard to therapy monitoring, it is of tremendous interest to understand associations between ATN biomarkers and neuroinflammation during the progressive aggregation of misfolded proteins in the brain. Thus, we also applied a model comprising all individual regional ATN biomarker data within groups of patients with 4RTs, typical AD, and atypical AD, again exploring the associations of the individual ATN biomarker adjusted for the remaining indices. Importantly, we found that, in a cross-sectional design, microglial activation still continuous to rise coupled with increasing tau pathology at stages with very high tau accumulation in primary and secondary tauopathies (Fig. 3). Contrary, TSPO-PET associations with regional Aβ aggregation tended to peak or plateau at stages of moderate Aβ abundance. This observation fits a recent study, suggesting that microglial activation correlates strongly with tau aggregation in established AD and with Aβ deposition in MCI [25]. Furthermore, two other studies indicated specific associations between Aβ and neuroinflammation at early stages of Aβ pathology [67, 68]. Thus, targeting tau associated microglial activation could still be beneficial at later stages of the disease, whereas modifying Aβ associated microglial activation may be only beneficial at early disease stages [48]. Understanding differences in microglia phenotypes associated either with Aβ or

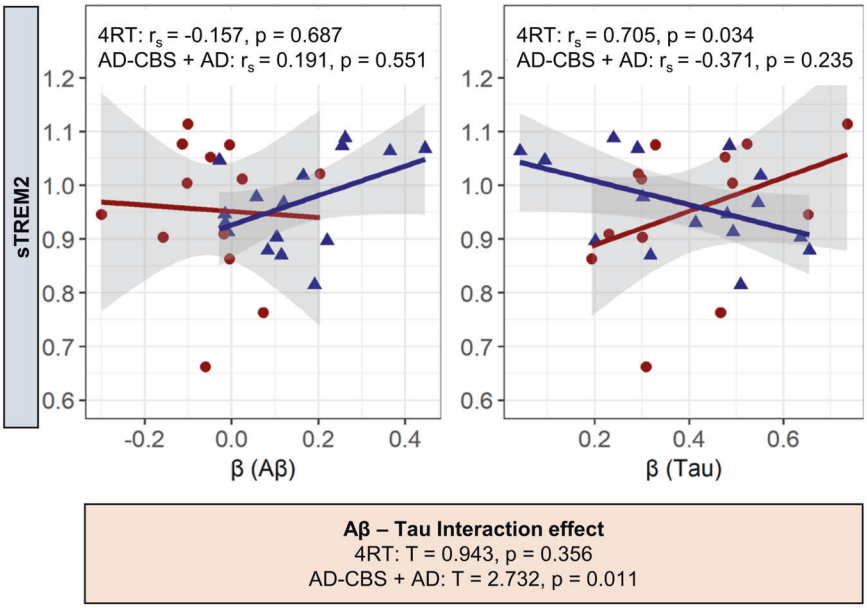

Fig. 5 Correlation of ATN associated microglial activation with sTREM2. Standardized coefficients β (single patient regression), to detect Aβ (A)- and tau (T)-associated microglial activation, were correlated with sTREM2 data (Spearman's correlation coefficient, r_s). The statistical analysis was calculated for the combined AD group (AD-CBS + AD), and the 4RT group. ● = 4RT, ▲ = AD-CBS + AD. Correlation analyses were adjusted for sex, age, global-patient-TSPO-load (mean z-scores of 246 VOIs), and global-patient-AT-load (mean z-scores of 246 VOIs of the respective biomarker). No correction for multiple testing was applied. Subsequently, A and T were tested for interaction effects. AD Alzheimer's disease, AD-CBS corticobasal syndrome with AD-pathology, 4RT four-repeat tauopathies, LAB low affinity binder, CTRL healthy controls, TSPO 18-kDa translocator protein, Aβ β-amyloid, GMV gray-matter-volume, sTREM2 soluble triggering receptor expressed on myeloid cells 2, PSPRS Progressive-Supranuclear-Palsy-Rating-Scale, MMSE Mini-Mental State Examination.

tau aggregation will likely have a major impact on selection of appropriate immunomodulatory strategies.

The relevance of regression models at the individual patient level was pinpointed by the observation of distinct heterogeneity of regional ATN biomarker alterations in patients with 4RTs and AD. In line, four distinct trajectories of tau deposition were recently identified in typical AD, which implies that pathology originates and spreads through distinct networks in the different subtypes [59, 66]. Distinct regional patterns of neurodegeneration were similarly reported for 4RTs [69]. This heterogeneity implies that conservative regional assessments at the group level limit the possibility to capture the full picture of ATN biomarker alterations because effects in single regions are diminished by differing regional peaks of pathology.

An exploratory analysis of our study suggested that strong regional associations between tau and microglial activation indicated worse clinical performance at a cross-sectional level of analysis in patients with primary and secondary tauopathies. This finding is in line with improved cognition in tauopathy models with NLRP3 inflammasome knock-out [70]. In contrast, the individual regional association of microglial activation with Aβ showed a more beneficial effect on clinical performance indices in patients with AD. Supporting this claim, levels of sTREM2 were specifically associated with Aβ related but not tau related microglial activation in our cohort, while sTREM2 was reported to be associated with reduced cognitive decline in AD [71]. In this regard, TREM2 may slow AD progression and reduce tau-driven neurodegeneration by restricting the degree to which β-amyloid facilitates the spreading of pathogenic tau [72]. Our observations also had similarities to serial preclinical studies in mouse models, where microglial activation was correlated with worse outcome parameters in the P301S tau model [61], but with improved spatial learning performance in PS2APP [73, 74] and $App^{NL\text{-}G\text{-}F}$ [17] Aβ models. A clinical study in patients with AD also suggested that anterior temporal [^{11}C]PK11195 binding, a region with abundant tau but low Aβ deposition is associated with progressive cognitive decline [75]. In this regard, our individual index of tau- and Aβ-associated microglia activation could serve to account for regional heterogeneity and standardized quantification of the multidimensional neuroinflammatory response. This may enable stratification for immunomodulatory therapies by identification of patients with a high risk of future clinical deterioration [75].

The characteristics of the used molecular imaging biomarkers for the assessment of ATI(N) need to be considered for the interpretation of our results. A strength of this study is given by the use of the novel tau-PET tracer [^{18}F]PI-2620 which proved absent of off-target binding to monoamine oxidases [76], high affinity to 3/4R-tau in AD [77] and also high affinity to recombinant 4R tau fibrils and PSP brain homogenate [76]. Colocalization of [^{18}F]PI-2620 binding with 4R tau in micro-autoradiography [76] and quantitative agreement of autoradiography and immunohistochemistry [66, 78] as well as in vivo discrimination of PSP [21] and CBS [4] from controls highlight the potential of this radioligand. Since currently available tau-PET tracers were optimized to detect AD-related tau tangles, the used tau-PET tracer shows differential binding characteristics to different tau isoforms, which is relevant in the described patient cohorts. Predominant 3/4R tau isoforms of patients with AD patients comprise favorable energetic and kinetic properties with regard to [^{18}F]PI-2620 binding, compared to predominant 4 R tau isoforms of primary tauopathies [79]. In this regard, [^{18}F]PI-2620 showed higher specificity to 4R tau in comparison to other second-generation tau-PET tracers in vitro [80]. In consideration of stronger binding to AD-related tau tangles compared to 4R-tau aggregates in primary tauopathies, the availability of a tau tracer with higher affinity to non-AD tau could even lead to stronger tau-related effects in the group of patients with 4R-tauopathies. Furthermore, early-phase [^{18}F]PI-2620 PET indicated feasibility for perfusion surrogate imaging in patients with AD and 4RTs [35, 43], which was applied as an "N" biomarker in the current study. [^{18}F] flutemetamol is an FDA and EMA approved Aβ-PET tracer and is characterized by fast brain uptake, fast clearance, and excellent

binding properties to Aβ deposits in vitro and in vivo [81]. TSPO-PET represents a sensitive biomarker for monitoring immunomodulation and can act as a surrogate for activated microglia. Several TSPO radioligands allow monitoring neuroinflammation in AD and 4R-tauopathies [18] and we were able to show that [^{18}F]GE-180 recapitulates the expected topology of microglial activation in 4RTs [22] and AD [33]. However, [^{18}F]GE-180 has recently been criticized for limited uptake across the blood-brain-barrier [22, 82] since blood-brain integrity can be disturbed in neurodegenerative disorders with a potential impact on tracer kinetics [83, 84]. We circumvented blood-brain-barrier related perfusion alterations and interrogated them as a potential cofounder by the inclusion of a perfusion surrogate as an "N" biomarker into our regression model. With this approach, we were able to show that perfusion has a substantial impact on [^{18}F]GE-180 binding, but our model also allowed us to determine the specific perfusion-adjusted impact of tau and Aβ pathology on TSPO-PET signal alterations. More importantly, we were able to show that associations between regional tau and Aβ accumulation with microglial activity were lost in low-affinity-binders. Furthermore, regional TSPO-PET signals were distinctly lower in participants with low-affinity binding status when compared to medium and high affinity binders. Thus, our data provide evidence of the specificity of the [^{18}F]GE-180 TSPO-PET signal in patients with neurodegenerative diseases.

Limitations of the study include that we cannot draw detailed conclusions about the cell type specificity of the TSPO-PET signal to activated microglia, since we did not measure associations with reactive astrocytosis by glial fibrillary acidic protein or a PET radioligand targeting reactive astrocytes. Furthermore, our study enrolled patients based on state-of-the-art clinical diagnosis but was not enriched by neuropathological confirmation. Thus, although the characterization of our patients was based on several biomarkers and detailed clinical work-up, misdiagnosed patients need to be considered as potential confounders in this study population.

CONCLUSION

A multi-regional regression model of PET and grey matter volume can serve for a personalized assessment of specific "A (Amyloid) T (Tau) and N (Neurodegeneration)" related microglial response rates. Tau pathology dominates the regional associations of these ATN biomarkers with microglial activation in primary and secondary tauopathies, while strong regional heterogeneity of ATN biomarker alterations needs to be considered at the individual patient level. Tau and Aβ related microglial response indices showed differential associations with cognitive performance and sTrem2-levels and may serve as a two-dimensional index for in vivo assessment of neuroinflammation in neurodegenerative diseases.

AVAILABILITY OF DATA AND MATERIALS

The datasets used and/or analyzed during the current study are available from the corresponding author upon reasonable request. Supplementary information is available on MP's website.

REFERENCES

1. Ziegler-Graham K, Brookmeyer R, Johnson E, Arrighi HM. Worldwide variation in the doubling time of Alzheimer's disease incidence rates. Alzheimers Dement. 2008;4:316–23.
2. Selkoe DJ, Hardy J. The amyloid hypothesis of Alzheimer's disease at 25 years. EMBO Mol Med. 2016;8:595–608.
3. Kovacs GG. Invited review: neuropathology of tauopathies: principles and practice. Neuropathol Appl Neurobiol. 2015;41:3–23.
4. Palleis C, Brendel M, Finze A, Weidinger E, Botzel K, Danek A, et al. Cortical [(18) F] PI-2620 binding differentiates corticobasal syndrome subtypes. Mov Disord. 2021;36:2104–15.
5. Braak H, Braak E. Demonstration of amyloid deposits and neurofibrillary changes in whole brain sections. Brain Pathol. 1991;1:213–6.
6. Hyman BT, Phelps CH, Beach TG, Bigio EH, Cairns NJ, Carrillo MC, et al. National Institute on Aging-Alzheimer's Association guidelines for the neuropathologic assessment of Alzheimer's disease. Alzheimers Dement. 2012;8:1–13.
7. Serrano-Pozo A, Frosch MP, Masliah E, Hyman BT. Neuropathological alterations in Alzheimer disease. Cold Spring Harb Perspect Med. 2011;1:a006189.
8. Querfurth HW, LaFerla FM. Alzheimer's disease. N Engl J Med. 2010;362:329–44.
9. Heneka MT, Carson MJ, Khoury JE, Landreth GE, Brosseron F, Feinstein DL, et al. Neuroinflammation in Alzheimer's disease. The Lancet Neurology. 2015;14:388–405.
10. Tan MS, Ji X, Li JQ, Xu W, Wang HF, Tan CC, et al. Longitudinal trajectories of Alzheimer's ATN biomarkers in elderly persons without dementia. Alzheimers Res Ther. 2020;12:55.
11. Hampel H, Cummings J, Blennow K, Gao P, Jack CR Jr., Vergallo A. Developing the ATX(N) classification for use across the Alzheimer disease continuum. Nat Rev Neurol. 2021;17:580–9.
12. Pascoal TA, Benedet AL, Ashton NJ, Kang MS, Therriault J, Chamoun M, et al. Microglial activation and tau propagate jointly across Braak stages. Nat Med. 2021;27:1592–9.
13. Ishizawa K, Dickson DW. Microglial activation parallels system degeneration in progressive supranuclear palsy and corticobasal degeneration. J Neuropathol Exp Neurol. 2001;60:647–57.
14. Villemagne VL, Burnham S, Bourgeat P, Brown B, Ellis KA, Salvado O, et al. Amyloid beta deposition, neurodegeneration, and cognitive decline in sporadic Alzheimer's disease: a prospective cohort study. Lancet Neurol. 2013;12:357–67.
15. Serrano-Pozo A, Mielke ML, Gomez-Isla T, Betensky RA, Growdon JH, Frosch MP, et al. Reactive glia not only associates with plaques but also parallels tangles in Alzheimer's disease. Am J Pathol. 2011;179:1373–84.
16. Werry EL, Bright FM, Piguet O, Ittner LM, Halliday GM, Hodges JR, et al. Recent developments in TSPO PET imaging as a biomarker of neuroinflammation in neurodegenerative disorders. Int J Mol Sci. 2019;20.
17. Biechele G, Blume T, Deussing M, Zott B, Shi Y, Xiang X, et al. Pre-therapeutic microglia activation and sex determine therapy effects of chronic immunomodulation. Theranostics. 2021;11:8964–76.
18. Cumming P, Burgher B, Patkar O, Breakspear M, Vasdev N, Thomas P, et al. Sifting through the surfeit of neuroinflammation tracers. J Cereb Blood Flow Metab. 2018;38:204–24.
19. Stefaniak J, O'Brien J. Imaging of neuroinflammation in dementia: a review. J Neurol Neurosurg Psychiatry. 2016;87:21–8.
20. Malpetti M, Passamonti L, Jones PS, Street D, Rittman T, Fryer TD, et al. Neuroinflammation predicts disease progression in progressive supranuclear palsy. J Neurol Neurosurg Psychiatry. 2021;92:769–75.
21. Brendel M, Barthel H, van Eimeren T, Marek K, Beyer L, Song M, et al. Assessment of 18F-PI-2620 as a biomarker in progressive supranuclear palsy. JAMA Neurol. 2020;77:1408–19.
22. Palleis C, Sauerbeck J, Beyer L, Harris S, Schmitt J, Morenas-Rodriguez E, et al. In Vivo assessment of neuroinflammation in 4-repeat tauopathies. Mov Disord. 2021;36:883–94.
23. Jecmenica Lukic M, Kurz C, Respondek G, Grau-Rivera O, Compta Y, Gelpi E, et al. Copathology in progressive supranuclear palsy: does it matter? Mov Disord. 2020;35:984–93.
24. Heneka MT, Kummer MP, Latz E. Innate immune activation in neurodegenerative disease. Nat Rev Immunol. 2014;14:463–77.
25. Dani M, Wood M, Mizoguchi R, Fan Z, Walker Z, Morgan R, et al. Microglial activation correlates in vivo with both tau and amyloid in Alzheimer's disease. Brain. 2018;141:2740–54.
26. Biel D, Suárez-Calvet M, Hager P, Rubinski A, Dewenter A, Steward A, et al. sTREM2 is associated with amyloidrelated p-tau increases and glucose hypermetabolism in Alzheimer's disease. EMBO Mol Med. 2023;15:e16987.
27. Su L, Surendranathan A, Huang Y, Bevan-Jones WR, Passamonti L, Hong YT, et al. Relationship between tau, neuroinflammation and atrophy in Alzheimer's disease: The NIMROD study. Inf Fusion. 2021;67:116–24.
28. Frigerio I, Boon BDC, Lin CP, Galis-de Graaf Y, Bol J, Preziosa P, et al. Amyloid-beta, p-tau and reactive microglia are pathological correlates of MRI cortical atrophy in Alzheimer's disease. Brain Commun. 2021;3:fcab281.
29. Jack CR Jr., Bennett DA, Blennow K, Carrillo MC, Dunn B, Haeberlein SB, et al. NIA-AA research framework: toward a biological definition of Alzheimer's disease. Alzheimers Dement. 2018;14:535–62.
30. Hoglinger GU, Respondek G, Stamelou M, Kurz C, Josephs KA, Lang AE, et al. Clinical diagnosis of progressive supranuclear palsy: the movement disorder society criteria. Mov Disord. 2017;32:853–64.
31. Armstrong MJ, Litvan I, Lang AE, Bak TH, Bhatia KP, Borroni B, et al. Criteria for the diagnosis of corticobasal degeneration. Neurology. 2013;80:496–503.

32. Palleis C, Sauerbeck J, Beyer L, Harris S, Schmitt J, Morenas-Rodriguez E, et al. In Vivo Assessment of Neuroinflammation in 4-Repeat Tauopathies. Mov Disord. 2021;36:883–94.
33. Rauchmann BS, Brendel M, Franzmeier N, Trappmann L, Zaganjori M, Ersoezlue E, et al. Microglial Activation and Connectivity in Alzheimer Disease and Aging. Ann Neurol. 2022;92:768–81.
34. Schmitt J, Palleis C, Sauerbeck J, Unterrainer M, Harris S, Prix C, et al. Dual-Phase beta-Amyloid PET Captures Neuronal Injury and Amyloidosis in Corticobasal Syndrome. Front Aging Neurosci. 2021;13:661284.
35. Beyer L, Nitschmann A, Barthel H, van Eimeren T, Unterrainer M, Sauerbeck J, et al. Early-phase [(18)F]PI-2620 tau-PET imaging as a surrogate marker of neuronal injury. Eur J Nucl Med Mol Imaging. 2020;47:2911–22.
36. Wollenweber FA, Darr S, Muller C, Duering M, Buerger K, Zietemann V, et al. Prevalence of amyloid positron emission tomographic positivity in poststroke mild cognitive impairment. Stroke. 2016;47:2645–8.
37. Song M, Scheifele M, Barthel H, van Eimeren T, Beyer L, Marek K, et al. Feasibility of short imaging protocols for [(18)F]PI-2620 tau-PET in progressive supranuclear palsy. Eur J Nucl Med Mol Imaging. 2021;48:3872–85.
38. Volter F, Beyer L, Eckenweber F, Scheifele M, Bui N, Patt M, et al. Assessment of perfusion deficit with early phases of [(18)F]PI-2620 tau-PET versus [(18)F]flutemetamol-amyloid-PET recordings. Eur J Nucl Med Mol Imaging. 2023;50:1384–94.
39. Lyoo CH, Ikawa M, Liow JS, Zoghbi SS, Morse CL, Pike VW, et al. Cerebellum can serve as a pseudo-reference region in alzheimer disease to detect neuroinflammation measured with PET radioligand binding to translocator protein. J Nucl Med. 2015;56:701–6.
40. Cho SH, Choe YS, Park S, Kim YJ, Kim HJ, Jang H, et al. Appropriate reference region selection of (18)F-florbetaben and (18)F-flutemetamol beta-amyloid PET expressed in Centiloid. Sci Rep. 2020;10:14950.
41. Fan L, Li H, Zhuo J, Zhang Y, Wang J, Chen L, et al. The human brainnetome atlas: a new brain atlas based on connectional architecture. Cereb Cortex. 2016;26:3508–26.
42. Kolabas ZI, Kuemmerle LB, Perneczky R, Förstera B, Büttner M, Caliskan OS, et al. Multi-omics and 3D-imaging reveal bone heterogeneity and unique calvaria cells in neuroinflammation. Cell. 2023. In press.
43. Katzdobler S, Nitschmann A, Barthel H, Bischof G, Beyer L, Marek K, et al. Additive value of [(18)F]PI-2620 perfusion imaging in progressive supranuclear palsy and corticobasal syndrome. Eur J Nucl Med Mol Imaging. 2023;50:423–34.
44. Owen DR, Gunn RN, Rabiner EA, Bennacef I, Fujita M, Kreisl WC, et al. Mixed-affinity binding in humans with 18-kDa translocator protein ligands. J Nucl Med. 2011;52:24–32.
45. Owen DR, Yeo AJ, Gunn RN, Song K, Wadsworth G, Lewis A, et al. An 18-kDa translocator protein (TSPO) polymorphism explains differences in binding affinity of the PET radioligand PBR28. J Cereb Blood Flow Metab. 2012;32:1–5.
46. Kleinberger G, Yamanishi Y, Suarez-Calvet M, Czirr E, Lohmann E, Cuyvers E, et al. TREM2 mutations implicated in neurodegeneration impair cell surface transport and phagocytosis. Sci Transl Med. 2014;6:243ra86.
47. Suarez-Calvet M, Morenas-Rodriguez E, Kleinberger G, Schlepckow K, Araque Caballero MA, Franzmeier N, et al. Early increase of CSF sTREM2 in Alzheimer's disease is associated with tau related-neurodegeneration but not with amyloid-beta pathology. Mol Neurodegener. 2019;14:1.
48. Morenas-Rodriguez E, Li Y, Nuscher B, Franzmeier N, Xiong C, Suarez-Calvet M, et al. Soluble TREM2 in CSF and its association with other biomarkers and cognition in autosomal-dominant Alzheimer's disease: a longitudinal observational study. Lancet Neurol. 2022;21:329–41.
49. Golbe LI, Ohman-Strickland PA. A clinical rating scale for progressive supranuclear palsy. Brain. 2007;130:1552–65.
50. Goetz CG, Tilley BC, Shaftman SR, Stebbins GT, Fahn S, Martinez-Martin P, et al. Movement disorder society-sponsored revision of the unified parkinson's disease rating scale (MDS-UPDRS): scale presentation and clinimetric testing results. Mov Disord. 2008;23:2129–70.
51. Sheikh J, Yesavage JA. Geriatric depression scale (GDS): recent evidence and development of a shorter version. Clin Gerontol. 1986;5:165–73.
52. Nasreddine ZS, Phillips NA, Bédirian V, Charbonneau S, Whitehead V, Collin I, et al. The Montreal cognitive assessment, MoCA: a brief screening tool for mild cognitive impairment. J Am Geriatr Soc. 2005;53:695–9.
53. Folstein MF, Folstein SE, McHugh PR. "Mini-mental state". A practical method for grading the cognitive state of patients for the clinician. J Psychiatr Res. 1975;12:189–98.
54. Bergeron D, Flynn K, Verret L, Poulin S, Bouchard RW, Bocti C, et al. Multicenter validation of an MMSE-MoCA conversion table. J Am Geriatr Soc. 2017;65:1067–72.
55. Vettermann FJ, Harris S, Schmitt J, Unterrainer M, Lindner S, Rauchmann BS, et al. Impact of TSPO Receptor Polymorphism on [(18)F]GE-180 Binding in Healthy Brain and Pseudo-Reference Regions of Neurooncological and Neurodegenerative Disorders. Life (Basel). 2021;11:484.
56. Metz CE. Basic principles of ROC analysis. Semin Nucl Med. 1978;8:283–98.
57. Vermont J, Bosson J-L, François P, Robert C, Rueff A, Demongeot J. Strategies for graphical threshold determination. Comput Methods Programs Biomed. 1991;35:141–50.
58. Brainnetome parcellation (http://atlas.brainnetome.org/bnatlas.html).
59. Vogel JW, Young AL, Oxtoby NP, Smith R, Ossenkoppele R, Strandberg OT, et al. Four distinct trajectories of tau deposition identified in Alzheimer's disease. Nat Med. 2021;27:871–81.
60. Kreisl WC. Discerning the relationship between microglial activation and Alzheimer's disease. Brain. 2017;140:1825–8.
61. Eckenweber F, Medina-Luque J, Blume T, Sacher C, Biechele G, Wind K, et al. Longitudinal TSPO expression in tau transgenic P301S mice predicts increased tau accumulation and deteriorated spatial learning. J Neuroinflammation. 2020;17:208.
62. Zou J, Tao S, Johnson A, Tomljanovic Z, Polly K, Klein J, et al. Microglial activation, but not tau pathology, is independently associated with amyloid positivity and memory impairment. Neurobiol Aging. 2020;85:11–21.
63. Wang WY, Tan MS, Yu JT, Tan L. Role of pro-inflammatory cytokines released from microglia in Alzheimer's disease. Ann Transl Med. 2015;3:136.
64. Bamberger ME, Harris ME, McDonald DR, Husemann J, Landreth GE. A cell surface receptor complex for fibrillar beta-amyloid mediates microglial activation. J Neurosci. 2003;23:2665–74.
65. Blume T, Focke C, Peters F, Deussing M, Albert NL, Lindner S, et al. Microglial response to increasing amyloid load saturates with aging: a longitudinal dual tracer in vivo muPET-study. J Neuroinflammation. 2018;15:307.
66. Franzmeier N, Brendel M, Beyer L, Slemann L, Kovacs GG, Arzberger T, et al. Tau deposition patterns are associated with functional connectivity in primary tauopathies. Nat Commun. 2022;13:1362.
67. Ismail R, Parbo P, Madsen LS, Hansen AK, Hansen KV, Schaldemose JL, et al. The relationships between neuroinflammation, beta-amyloid and tau deposition in Alzheimer's disease: a longitudinal PET study. J Neuroinflammation. 2020;17:151.
68. Toppala S, Ekblad LL, Tuisku J, Helin S, Johansson JJ, Laine H, et al. Association of early beta-amyloid accumulation and neuroinflammation measured with [(11)C]PBR28 in elderly individuals without dementia. Neurology. 2021;96:e1608–e19.
69. Beyer L, Meyer-Wilmes J, Schonecker S, Schnabel J, Brendel E, Prix C, et al. Clinical routine FDG-PET imaging of suspected progressive supranuclear palsy and corticobasal degeneration: a gatekeeper for subsequent Tau-PET imaging? Front Neurol. 2018;9:483.
70. Ising C, Venegas C, Zhang S, Scheiblich H, Schmidt SV, Vieira-Saecker A, et al. NLRP3 inflammasome activation drives tau pathology. Nature. 2019;575:669–73.
71. Ewers M, Franzmeier N, Suárez-Calvet M, Morenas-Rodriguez E, Caballero MAA, Kleinberger G, et al. Increased soluble TREM2 in cerebrospinal fluid is associated with reduced cognitive and clinical decline in Alzheimer's disease. Sci Transl Med. 2019;11:eaav6221.
72. Lee SH, Meilandt WJ, Xie L, Gandham VD, Ngu H, Barck KH, et al. Trem2 restrains the enhancement of tau accumulation and neurodegeneration by β-amyloid pathology. Neuron. 2021;109:1283–301.e6.
73. Focke C, Blume T, Zott B, Shi Y, Deussing M, Peters F, et al. Early and longitudinal microglial activation but not amyloid accumulation predicts cognitive outcome in PS2APP mice. J Nucl Med. 2019;60:548–54.
74. Blume T, Deussing M, Biechele G, Peters F, Zott B, Schmidt C, et al. Chronic PPARgamma stimulation shifts amyloidosis to higher fibrillarity but improves cognition. Front Aging Neurosci. 2022;14:854031.
75. Malpetti M, Kievit RA, Passamonti L, Jones PS, Tsvetanov KA, Rittman T, et al. Microglial activation and tau burden predict cognitive decline in Alzheimer's disease. Brain. 2020;143:1588–602.
76. Kroth H, Oden F, Molette J, Schieferstein H, Capotosti F, Mueller A, et al. Discovery and preclinical characterization of [(18)F]PI-2620, a next-generation tau PET tracer for the assessment of tau pathology in Alzheimer's disease and other tauopathies. Eur J Nucl Med Mol Imaging. 2019;46:2178–89.
77. Mueller A, Bullich S, Barret O, Madonia J, Berndt M, Papin C, et al. Tau PET imaging with (18)F-PI-2620 in patients with Alzheimer disease and healthy controls: a first-in-humans study. J Nucl Med. 2020;61:911–9.
78. Willroider M, Roeber S, Horn AKE, Arzberger T, Scheifele M, Respondek G, et al. Superiority of formalin-fixed paraffin-embedded brain tissue for in vitro assessment of progressive supranuclear palsy tau pathology with [(18) F]PI-2620. Front Neurol. 2021;12:684523.
79. Kunze G, Kumpfel R, Rullmann M, Barthel H, Brendel M, Patt M, et al. Molecular simulations reveal distinct energetic and kinetic binding properties of [(18)F]PI-2620 on Tau filaments from 3R/4R and 4R Tauopathies. ACS Chem Neurosci. 2022;13:2222–34.
80. Malarte ML, Gillberg PG, Kumar A, Bogdanovic N, Lemoine L, Nordberg A. Discriminative binding of tau PET tracers PI2620, MK6240 and RO948 in Alzheimer's disease, corticobasal degeneration and progressive supranuclear palsy brains. Mol Psychiatry. 2023;28:1272–83.

81. Snellman A, Rokka J, Lopez-Picon FR, Eskola O, Wilson I, Farrar G, et al. Pharmacokinetics of [(1)(8)F]flutemetamol in wild-type rodents and its binding to beta amyloid deposits in a mouse model of Alzheimer's disease. Eur J Nucl Med Mol Imaging. 2012;39:1784–95.
82. Zanotti-Fregonara P, Pascual B, Rostomily RC, Rizzo G, Veronese M, Masdeu JC, et al. Anatomy of (18)F-GE180, a failed radioligand for the TSPO protein. Eur J Nucl Med Mol Imaging. 2020;47:2233–6.
83. van Assema DM, Lubberink M, Bauer M, van der Flier WM, Schuit RC, Windhorst AD, et al. Blood-brain barrier P-glycoprotein function in Alzheimer's disease. Brain. 2012;135:181–9.
84. de Vries HE, Kuiper J, de Boer AG, Van Berkel TJ, Breimer DD. The blood-brain barrier in neuroinflammatory diseases. Pharmacol Rev. 1997;49:143–55.

AUTHOR CONTRIBUTIONS

(1) Research project: (A) Conception: AF, GB, AR, PB, RP, CH, JL, GUH, and MB. (B) Organization: AF, GB, AR, PB, RP, CH, JL, GUH, and MB. (C) Execution: BR, SSc, SH, JS, LB, JG, SL, NLA, DK, SSt, and OD performed human PET and MRI scans and their analysis. CP, SK, EW, SG, KB, AD, LB, CK, MT, JU, BP, MZ, LT, OG, TG, JH, DJ, BR, RP, MS, PB, JL and GH recruited patients, examined patients and controls. SL, PB, HB, and OS contributed to tracer synthesis and delivery. (2) Statistical Analysis: (A) Design: AF, GB, NF, EW, CP, KB, AD, BR, RP, JL, GUH and MB designed analysis of clinical data. (B) Execution: NF, EW, CP, KB, AD, BR, RP, JL, GH and MB analyzed clinical data. EM and CH performed sTREM2 analysis. NLA, CW and RR performed TSPO polymorphism analysis. AF, GB, LB, PB and MB interpreted human PET data. (C) Review and Critique: all authors. (3) Manuscript Preparation: (A) Writing of the first draft: AF, GB and MB. (B) Review and Critique: all authors.

FUNDING

This work was supported by grants from the Deutsche Forschungsgemeinschaft (DFG, German Research Foundation) under Germany's Excellence Strategy within the framework of the Munich Cluster for Systems Neurology (EXC 2145 SyNergy – ID 390857198) and within research units (FOR-2858 project numbers 403161218, 421887978, 422188432, 422182557 and 422179811). GUH was funded by the Hannover Cluster RESIST (EXC 2155 – project number 39087428), the German Federal Ministry of Education and Research (BMBF, 01KU1403A EpiPD; 01EK1605A HitTau; 01DH18025 TauTherapy); European Joint Programme on Rare Diseases (Improve-PSP); Deutsche Forschungsgemeinschaft (DFG, HO2402/18-1 MSAomics), VolkswagenStiftung (Niedersächsisches Vorab); Petermax-Müller Foundation (Etiology and Therapy of Synucleinopathies and Tauopathies). The Lüneburg Heritage and Friedrich-Baur-Stiftung have supported the work of CP. SK was supported by Ehrmann Foundation and Lüneburg Heritage. The Alzheimer Forschung Initiative e.V. provided grant no. 19063p to MB. The Hirnliga e.V. supported recruitment and imaging of the ActiGliA cohort (Manfred-Strohscheer-Stiftung) by a grant to BSR and MB. RP was supported by the Davos Alzheimer's Collaborative, the VERUM Foundation, the Robert-Vogel-Foundation, the National Institute for Health and Care Research (NIHR) Sheffield Biomedical Research Centre (NIHR203321), the University of Cambridge - Ludwig-Maximilians-University Munich Strategic Partnership within the framework of the German Excellence Initiative and Excellence Strategy and the European Commission under the Innovative Health Initiative program (project 101132356). Open Access funding enabled and organized by Projekt DEAL.

COMPETING INTERESTS

CH collaborates with Denali Therapeutics. CH is chief advisor of ISAR Bioscience and a member of the advisory board of AviadoBio. TG received consulting fees from AbbVie, Alector, Anavex, Biogen, Eli Lilly, Functional Neuromodulation, Grifols, Iqvia, Noselab, Novo Nordisk, NuiCare, Orphanzyme, Roche Diagnostics, Roche Pharma, UCB, and Vivoryon; lecture fees from Grifols, Medical Tribune, Novo Nordisk, Roche Pharma, and Schwabe; and has received grants to his institution from Roche Diagnostics. GUH participated in industry-sponsored research projects from Abbvie, Biogen, Biohaven, Novartis, Roche, Sanofi, UCB; serves as a consultant for Abbvie, Alzprotect, Aprineua, Asceneuron, Bial, Biogen, Biohaven, Kyowa Kirin, Lundbeck, Novartis, Retrotope, Roche, Sanofi, UCB; received honoraria for scientific presentations from Abbvie, Bayer Vital, Bial, Biogen, Bristol Myers Squibb, Kyowa Kirin, Roche, Teva, UCB, Zambon; holds a patent on Treatment of Synucleinopathies. United States Patent No.: US 10,918,628 B2: EP 17 787 904.6-1109 / 3 525 788; received publication royalties from Academic Press, Kohlhammer, and Thieme. MB received speaker honoraria from GE healthcare, Roche and LMI and is an advisor of LMI. LB is a Novartis Radiopharmaceuticals GmbH employee since 10/2022, unrelated to this work.

ADDITIONAL INFORMATION

Supplementary information The online version contains supplementary material available at https://doi.org/10.1038/s41380-023-02188-8.

Correspondence and requests for materials should be addressed to Matthias Brendel.

Reprints and permission information is available at http://www.nature.com/reprints

Publisher's note Springer Nature remains neutral with regard to jurisdictional claims in published maps and institutional affiliations.